# Cyber-physical Resilience Enhancement for Power Transmission Systems with Energy Storage Systems

Wenhao Zhang, Dongyang Rui, Weihong Wang, Yang Guo, Zhaoxia Jing, *Member*, *CSEE*, *Member*, *IEEE*, and Wenhu Tang, *Fellow*, *CSEE*, *Senior Member*, *IEEE*

***Abstract*—In a power system, when extreme events occur, such as ice storm, large scale blackouts may be unavoidable. Such small probability but high risk events have huge impact on power systems. Most resilience research in power systems only considers faults on the physical side, which would lead to overly idealistic results. This paper proposes a two-stage cyber-physical resilience enhancement method considering energy storage (ES) systems. The first stage calculates optimal planning of ES systems, and the second stage assesses resilience and enhancement of ES systems during the disaster. In the proposed model, cyber faults indirectly damage the system by disabling monitoring and control function of control center. As a result, when detection and response process of physical faults are blocked by cyber failures, serious load shedding occurs. Such a cyber-physical coupling mechanism of fault, response, restoration process is demonstrated in the modified IEEE Reliable Test System-79 (RTS-79). Simulation results show compared with the physical-only system, the cyber-physical system has a more accurate but degraded resilient performance. Besides, ES systems setting at proper place effectively enhance resilience of the cyber-physical transmission system with less load Shedding.**

***Index Terms*—Cyber-physical faults, energy storage systems, resilience enhancement, transmission systems.**

## I. Introduction

THE concept of resilience was firstly proposed by Professor C. S. Holling in 1973 to describe the ability of ecosystem to resist disturbance and maintain system stability. Then, it was introduced to environmental science [1] and economics [2]. As the largest and most complex energy system of human society, reliability of power system is particularly important. In 2009, U.S. smart grid report pointed out resilience is one of the characteristics of smart grid, which focuses on resilience under extreme events. There is no unified definition of resilient power system. However, from existing research, the meaning of resilient power system is basically the same, which is about prevention and resistance ability before disasters, emergency response ability during disasters, and rapid recovery ability after disasters [3], which is summarized as Fig. 1.

Current research on resilience of power systems can be divided into three categories: extreme event, resilience assessment, and resilience enhancement. First, extreme event models includes typhoon [4], ice storm [5], wildfire [6], thunderstorm [7], waterlogging [8], earthquake [9] etc. Second, resilient assessment and its quantification is the next step to describe impact during disasters. Based on extreme event model, there are two main assessment techniques, i.e. the Monte Carlo approach and Markov approach. The Monte Carlo simulation is a statistical experiment method using a large number of scenarios to capture component faults as weather evolves [10]–[12]. The Markov approach fully describes the sequential decision process considering uncertainty of each simulation period, regarding fault state of the system as a Markov state [13]–[15]. To quantify resilience, maximum of load reduction was taken as resilience index [16] and triangle based [17], trapezoid based [10] indexes were introduced. Third, based on resilient assessment above, corresponding improvement measure is defined as resilient enhancement. Before a disaster, components strengthen [12], day-ahead scheduling [4], planning of ES systems [18], [19] and mobile generators [20] were applied. During a disaster, proactive operation [14], network reconfiguration [21], optimization of mobile ES systems [22], [23] and re-routing installed mobile ES systems [18] were proposed; After a disaster, optimal repair sequence [24] and repair routing [5] were investigated. The research above only considers faults of a physical system, which may lead to inaccurate results.

Accidents of cyber faults on a physical system have already occurred. In reality, most protection and control signals are transmitted through Optical Ground Wire (OPGW), which is located at the top of transmission line. When OPGW fails during extreme weather, part of the system may become disconnected. For example, in 2016, typhoon Meranti hit the transmission network of Xiamen and caused the collapse of the 550 kV and 220 kV towers. Although the active and standby routing mechanism was applied for the optical transport network, under the influence of Meranti, the northwest cyber network was seriously damaged, and the fault of the system was further aggravated due to disconnection of generators with the control center. The above accident shows traditional physical-only resilient assessment is inaccurate and cyber faults indirectly affect the system.

Manuscript received November 2, 2022; revised January 16, 2023; accepted February 16, 2023. Date of online publication December 28, 2023; date of current version January 15, 2024. This work was supported by the Project funded by China Postdoctoral Science Foundation (Grant No.2022M710906).

W. H. Zhang, Z. X. Jing, and W. H. Tang (corresponding author, email: wenhutang@scut.edu.cn) are with School of Electric Power Engineering, South China University of Technology, Guangzhou 510640, China.

W. H. Zhang, D. Y. Rui, W. H. Wang, and Y. Guo are with Guangzhou Zhiguang Electric Co., Ltd and Zhiguang Research Institute (Guangzhou) Co., Ltd, Guangzhou 510765, China.

DOI: 10.17775/CSEEJPES.2022.07570

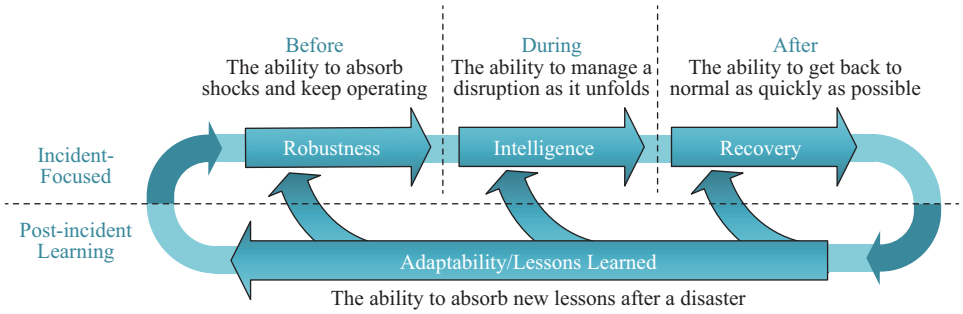


Fig. 1. Closed-loop process of extreme events.

Therefore, impacts of cyber fault on power system gradually draw attention of scholars. In [25], failure of monitoring and control function was modeled and analyzed, which focused on reliability assessment not resilient assessment. In [26], impact of cyber interruption on a wide-area protection system was studied and corresponding enhancement was given based on the combined contingency generated by corresponding risk indexes but not real disaster simulation. Since 2021, studies on cyber-physical power systems focused on the topic of resilience. A robust optimization method was proposed for communication network to distribute important messages on reliable links and improve cyber-physical resilience [27]. A cyber-physical resilience enhancement method was proposed in [28], including zone division before, power adjustment during and collaborative restoration after a disaster. A cyber-physical recovery strategy considering delay caused by cyber faults was proposed in [29]. It was pointed out the digital power system should consider cooperation of cyber and physical at the same time, and a comprehensive review of cyber-physical resilience was given in [30]. In [31], a two-stage cyber-physical resilient management incorporating ES systems and network reconfiguration was proposed against hurricanes, which were simplified to a vulnerability list.

In summary, there are two noticeable research gaps from the literature above. 1) Cyber-physical resilience has seldom been studied under a specific disaster model. Simulation with simple and constant fault probability or manually set fault sequence cannot reflect the time-space relation of the whole disaster process accurately [25]–[28]. 2) ES systems are efficient back-up resources during extreme events due to their automatic power support ability with no cyber network required. Research above improve resilience involving ES systems seldom consider impacts of cyber faults, which reduce damage of the system [18], [19], [22], [23].

### A. Innovation and contributions

Different from the physical-only resilience, this paper introduces cyber-physical coupling relationship and enhancement method involving ES systems. The main innovations and contributions of this paper are listed as the following.

1) The resilient process including fault model under a specific disaster, response model considering failure of monitoring and control, and the restoration model is proposed considering cyber-physical characteristic, which has not been studied before to the author's knowledge.

2) Configuration of ES systems is proposed as a resilience enhancement method in cyber-physical transmission system. The optimized power support function of ES systems with no communication required becomes the solution for power unbalance under cyber-physical faults.

3) Planning model of ES systems considering construction cost and operation cost is established, which is solved based on cyber-physical resilient process.

### B. Organization of This Paper

Figure 2 illustrates the organization of the rest of this paper: 1) Section II shows the background model including cyber-physical network, ice storm, and resilient indexes. 2) Sec-

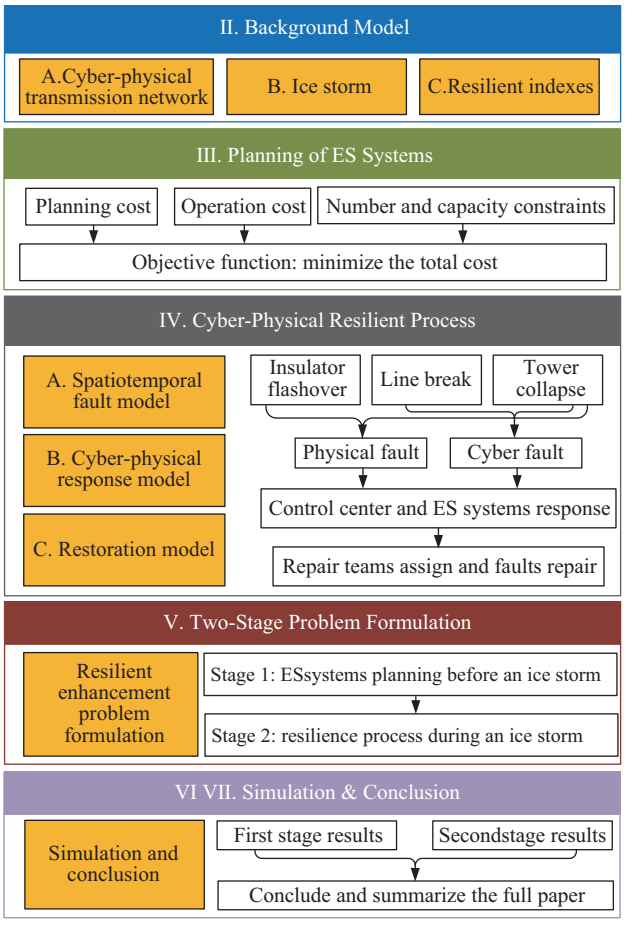


Fig. 2. Organization of the rest of this paper.

tion III describes planning model of ES systems. 3) Section IV proposes the cyber-physical resilient process including the spatiotemporal fault, response and restoration model. 4) The above resilience enhancement by planning ES systems is formulated as a two-stage problem illustrated in Section V. 5) Simulation and conclusion are given in Sections VI and VII.

## II. Background

### A. Cyber-physical Transmission Network

Considering the transmission network is large span with complex terrain and inconvenient transportation, it is uneconomic to set up another corridor for communication network. A practical way to save the space of transmission corridor is the OPGW, which is realized by embedding communication media, optical fiber, into the overhead ground wire. Using OPGW, cyber network of the transmission system has a similar topology with its physical network.

In this paper, the modified IEEE RTS-79 [32] is taken as an example to demonstrate a cyber-physical coupling network. Physical network and its corresponding cyber network are depicted in Fig. 3. There are 24 buses and 38 transmission lines in the physical network. Each bus represents a substation and corresponds to a communication node [33], [34]. Those buses connected with a transformer, such as bus 3 and 24, belong to the same substation and communication node. Node 8, the central node, acts as the control center of the test system, which is responsible for monitoring the operation state of the system and sending control command.

To analyze the impact of ice storm, cyber-physical network of IEEE RTS-79 is rasterized into $1600 \times 1800 = 2400000$ physical units and 2400000 cyber units with 500 m $\times$ 500 m areas as Fig. 4 shows, where the blue circle represents ice storm and blue arrows represent the path. For simplicity, in each unit, intensity of ice storm and the geographical position are assumed to be the same.

### B. Ice Storm

To evaluate catastrophic spatiotemporal damage of icing on the system, modeling ice storms is essential. First, the icing model is carried out. Then, multiple scenarios of ice storms based on the joint Probability Distribution Function (PDF) is given.

As shown in Fig. 5, blue radial shades represent affected range of ice storm, where the darker the color is, the more serious storm is. Yellow circles are maximum wind speed circles with radius $r_{\max}$ given in km. The blue dotted line is the path of ice storm. The green line represents power transmission wire and the red line represents the OPGW.

According to [35], thickness of a certain location can be calculated as follows.

$$R(t) = \int_0^t \frac{1}{\rho_i \pi} \sqrt{[P(t)\rho_0]^2 + [3.6v(t)W(t)]^2} \tag{1}$$

where $R(t)$ is ice thickness; $P(t)$ is precipitation of certain location, which is given in mm/h. Density of ice and water are set as $\rho_i = 0.9$ g/cm$^3$, $\rho_0 = 1$ g/cm$^3$ respectively. $v(t)$ is wind speed given in m/s and $W(t)$ is water content of atmosphere, where $W(t) = 0.72P(t)^{0.88}$.

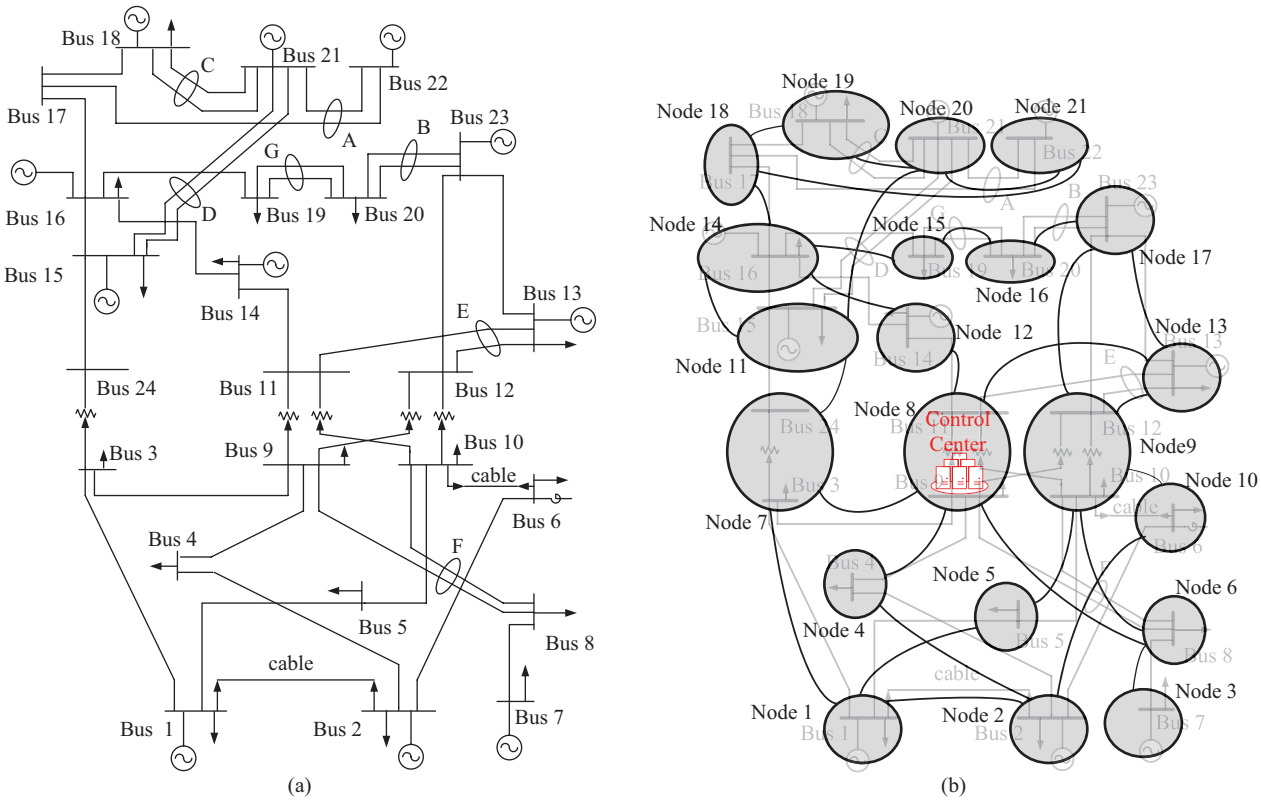


Fig. 3. Cyber-physical network of modified IEEE RTS-79. (a) Physical network. (b) Cyber network.

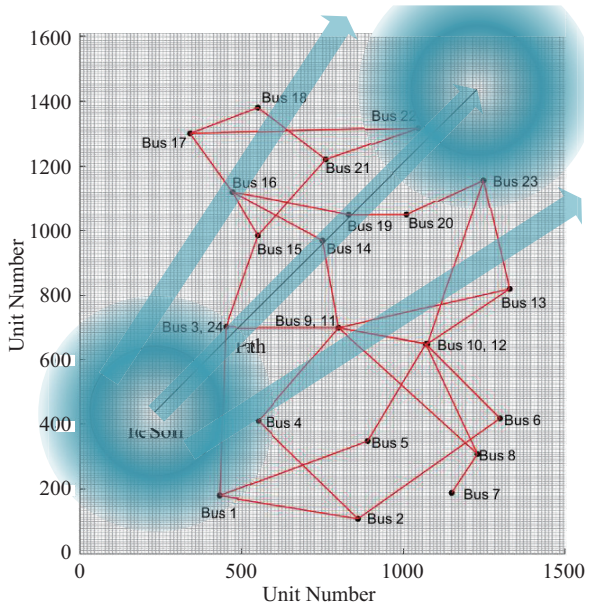


Fig. 4. Rasterization of IEEE RTS-79 under an ice storm.

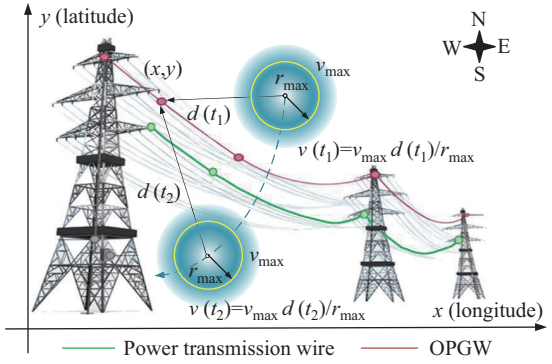


Fig. 5. Impacts of ice storm on power transmission wire and OPGW.

*1) Wind Speed*

Wind speed $v(t)$ of a certain location is given as [16]

$$v(t) = \begin{cases} v_{\max} d(t)/r_{\max}, & d(t) \le r_{\max} \\ v_{\max}[r_{\max}/d(t)]^{0.6}, & d(t) > r_{\max} \end{cases} \tag{2}$$

where $v_{\max}$ is the maximum wind speed, $d(t)$ is the distance to ice storm center, $r_{\max}$ is the diameter of maximum wind speed circle (yellow circle). $d(t)$ can be obtained by

$$d(t) = \sqrt{[x - x_{\mathrm{c}}(t)]^2 + [y - y_{\mathrm{c}}(t)]^2} \tag{3}$$

where $(x, y)$ are coordinates of a certain location and $(x_{\mathrm{c}}(t), y_{\mathrm{c}}(t))$ are that of the storm center.

*2) Precipitation*

Precipitation $P(t)$ has characteristic of attenuation, which is

$$P(t) = P_{\max}[r_{\max} - d(t)]/r_{\max}, \ d(t) \le r_{\max} \tag{4}$$

where $P_{\max}$ is the maximum precipitation of ice storm.

The icing model is carried out in (1)–(4). Uncertainties of ice storm are described by distributions of parameters, including maximum wind speed $v_{\max}$, maximum radius $r_{\max}$, maximum precipitation $P_{\max}$, moving speed $V_{\mathrm{m}}$, motion direction $\delta$, and landing site coordinates $(x_0, y_0)$. Take $v_{\max}$ as an example. According to [16], occurrence probability of $v_{\max} = v_s$ under ice storm $s$ is given as

$$P_{\mathrm{r}}(v_s) = \int_{v_s - c_H/2}^{v_s + c_H/2} f(v_{\max}) \mathrm{d}v_{\max} \tag{5}$$

where $P_{\mathrm{r}}()$ is probability of each parameter. $f()$ is probability density function, which is divided into several equal portions with interval $c_H$.

Therefore, occurrence probability of ice storm $s$ can be evaluated as the joint probability distribution of each parameter obtained by (6), as shown in Fig. 6.

$$P_s = P_{\mathrm{r}}(v_s) P_{\mathrm{r}}(r_s) P_{\mathrm{r}}(P_s) P_{\mathrm{r}}(V_s) P_{\mathrm{r}}(\delta_s) P_{\mathrm{r}}(x_{0,s}, y_{0,s}) \tag{6}$$

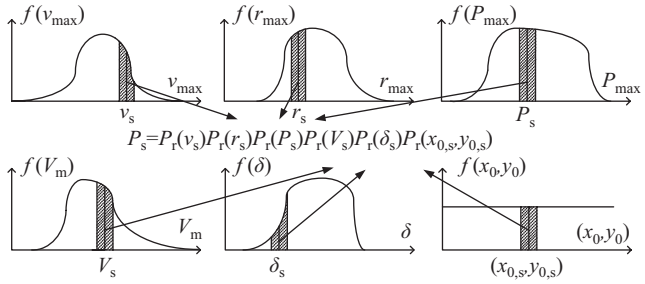


Fig. 6. The occurrence probability of ice storm $s$.

## C. Resilience Indexes

Resilience indexes are given according to system load during resilient process. The typical resilient curve is given in Fig. 7, where $X_1$ is the load of normal state and $X_2$ is the load of the most serious state. In Fig. 7, $T_0 - T_6$ are time when extreme event arrives, system begins load shedding, system load reach $X_1$, system begins restoration, extreme event passes through, system load returns to $X_2$, system fully recovers, respectively. $i(t)$ and $r(t)$ are ideal load curve if there is no extreme event and real load curve, respectively. $A_1 - A_4$ are corresponding areas set for description of resilient indexes, $R_{\mathrm{t}}$ [36], $R_{\mathrm{r}}$ [37], $R_{\mathrm{RICD}}$ [12].

$$R_{\mathrm{t}} = \int_{T_1}^{T_5} [i(t) - r(t)] \mathrm{d}t = A_3 \tag{7}$$

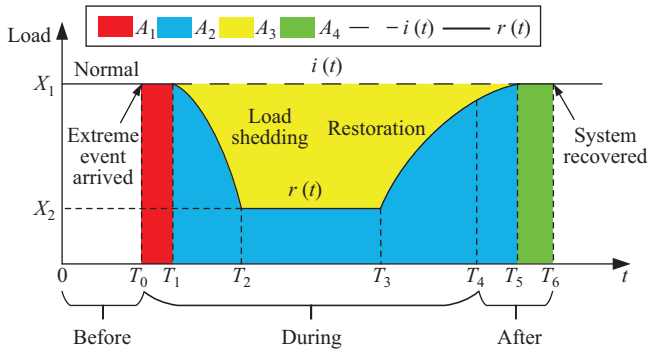


Fig. 7. Resilient curve under extreme events.

$$R_{\mathrm{r}}=\int_{T_1}^{T_5} r(t)\mathrm{d}t/\int_{T_1}^{T_5} i(t)\mathrm{d}t=A_2/(A_2+A_3) \tag{8}$$

$$R_{\mathrm{RICD}}=\frac{\int_{T_0}^{T_5} r(t)\mathrm{d}t}{\int_{T_0}^{T_5} i(t)\mathrm{d}t}\cdot\frac{T_4-T_0}{T_5-T_0}=\frac{A_1+A_2}{A_1+A_2+A_3}\cdot\frac{T_4-T_0}{T_5-T_0} \tag{9}$$

where $R_{\mathrm{t}}$ quantifies resilience by the area between ideal curve $i(t)$ and actual resilience curve $r(t)$, which can be interpreted as the load shedding area. Considering $R_{\mathrm{t}}$ is difficult to compare between different test systems, corresponding normalized index $R_{\mathrm{r}}$ is introduced, quantifying resilience by integral from $T_1$ to $T_5$ of $r(t)/i(t)$. Because $R_{\mathrm{t}}$ and $R_{\mathrm{t}}$ do not consider resistance ability of the system and restoration speed, which are $A_1$ and $(T_4-T_0)/(T_5-T_0)$ respectively, $R_{\mathrm{RICD}}$ is introduced.

## III. Planning of ES Systems

ES systems are quick response resources with hundreds of microseconds response speed, which are now considered to be part of relay protection of Shandong Province, China. By frequency detection of grid connection points, ES systems are able to take over load automatically during ice storm to avoid serious load shedding. Thus, employment of ES systems at weak points is an effective way to enhance resilience of the system. The objective of ES planning model is to minimize both construction cost and system operation cost during ice storm. The objective function is described as:

$$\min\left\{C_{\mathrm{ES}}^{\mathrm{plan}}+\sum_{s\in\Omega_s}\left[P_s\sum_{t\in T}\min(k_{\mathrm{g}}\cdot C_{t,s}^{\mathrm{System}})\right]\right\} \tag{10}$$

$$C_{\mathrm{ES}}^{\mathrm{plan}}=\sum_{i\in\mathcal{N}}(O_{\mathrm{ES}}^{i}C_{\mathrm{fix}}+E_{\mathrm{ES\_plan}}^{i}C_{\mathrm{cap}}) \tag{11}$$

where $C_{\mathrm{ES}}^{\mathrm{plan}}$ is the construction cost of ES systems. $\Omega_s$ is the set of sampled scenarios. $T$ is total time of ice storm. $C_{t,s}^{\mathrm{System}}$ is the system operation cost at time $t$ of scenario $s$, which is related to the resilient process detailed in Section IV. $k_{\mathrm{g}}$ is corresponding weight. $C_{\mathrm{fix}}$ is the fixed construction cost and $C_{\mathrm{cap}}$ is the capacity cost per MWh. $\mathcal{N}$ is the set of all buses of the system. $O_{\mathrm{ES}}^{i}$ is a boolean variable representing whether bus $i$ connects to storage energy (1 for connected, 0 for not). $E_{\mathrm{ES\_plan}}^{i}$ is a variable representing planning capacity of ES system at bus $i$.

The following constraints on the total number and capacity of ES systems are considered.

$$0\le\sum_{i\in\mathcal{N}}O_{\mathrm{ES}}^{i}\le N_{\mathrm{ES,set}} \tag{12}$$

$$0\le E_{\mathrm{ES\_plan}}^{i}\le O_{\mathrm{ES}}^{i}\cdot E_{\mathrm{ES\_max}}^{i},\ \forall i\in\mathcal{N} \tag{13}$$

where $N_{\mathrm{ES,set}}$ is the maximum planning number and $E_{\mathrm{ES\_max}}^{i}$ is maximum planning capacity of each ES system.

## IV. Cyber-Physical Resilient Process

Once the maximum ice carrying capacity is exceeded, part of the system is affected. Relying on the cyber network, the control center obtains current state of the system and responses with a certain control strategy. For those cyber disconnected areas, ES systems automatically output according to frequency of merging points and fill the load gap. Restoration begins after ice storm passes through. Such a cyber-physical fault, response and restoration model is the focus of this section.

### A. Spatiotemporal Fault Model

Since buses and substations have relatively higher protection levels than lines and towers, it is assumed faults only occur on lines and towers. For simplicity, each physical unit of the rasterization detailed in Section II-A is abstracted as an insulator element, a physical wire element and a tower element. Each cyber unit is abstracted as a cyber wire element and a tower element. Faults of these elements are modeled by an exponential fitting function [16] to described fault probability derived from geometrical and material nonlinearities [11], [12].

*1) Flashover of Insulator*

The increase of ice thickness on insulator reduces its insulation performance, which leads to flashover and causes line trip of physical network. The flashover fault rate is described as

$$\lambda_{\mathrm{F}}^{i}=\begin{cases}0, & U\le 0.8\hat{U}_{\mathrm{f}}\\ \exp\left[\frac{0.6931(U-0.8\hat{U}_{\mathrm{f}})}{0.8\hat{U}_{\mathrm{f}}}\right]-1, & 0.8\hat{U}_{\mathrm{f}}<U<\hat{U}_{\mathrm{f}}\\ 1, & U\ge\hat{U}_{\mathrm{f}}\end{cases} \tag{14}$$

where $U=220$ is operation voltage (kV). $\hat{U}_{\mathrm{f}}$ is flashover voltage, which is given as [38]

$$\hat{U}_{\mathrm{f}}=A\cdot R^{-c}\cdot h \tag{15}$$

where $A$ is a constant related to the pollution level, material and profile of the insulator; $c$ is the exponent characterizing influence of ice thickness on icing flashover voltage; $h$ is the dry arc distance given in meters. Assume FXBW-110/100 insulators are applied to the test system, there are $A=408.5$, $c=0.49$ and $h=3$.

*2) Disconnection of Physical/cyber Wire*

Over-weight of icing on the wire may damage the power transmission wire or the OPGW when it exceeds design value. According to [39], wire disconnection rate is given as

$$\lambda_{\mathrm{D}}^{i}=\begin{cases}0, & R\le\hat{R}_{\mathrm{w}}\\ \exp\left[\frac{0.6931(R-\hat{R}_{\mathrm{w}})}{4\hat{R}_{\mathrm{w}}}\right]-1, & \hat{R}_{\mathrm{w}}<R<5\hat{R}_{\mathrm{w}}\\ 1, & R\ge 5\hat{R}_{\mathrm{w}}\end{cases} \tag{16}$$

where $\hat{R}_{\mathrm{w}}$ is the design value of the ice thickness of the wire.

It is worth noting that the hanging point of OPGW is about 7 m higher than the power transmission wire and thus OPGW ices first when suffering from ice storm. Furthermore, different from power transmission wire, the OPGW does not heat and its temperature is almost equivalent to atmospheric temperature. Therefore, icing of OPGW is often more serious than that of the power transmission wire.

In this paper, transmission wire LGJ-630/45 and OPGW-150 are applied to test system with the $\hat{R}_{\mathrm{w}}=13$ and 15 respectively.

*3) Collapse of Tower*

The over weight of icing causes collapse of tower, interrupting both physical and cyber branches. The tower collapse rate is given as

$$\lambda_{\mathrm{C}}^{i}=\begin{cases}0, & R\le\hat{R}_{\mathrm{t}}\\ \exp\left[\frac{0.6931(R-\hat{R}_{\mathrm{t}})}{9\hat{R}_{\mathrm{t}}}\right]-1, & \hat{R}_{\mathrm{t}}<R<10\hat{R}_{\mathrm{t}}\\ 1, & R\ge 10\hat{R}_{\mathrm{t}}\end{cases}\tag{17}$$

where $\hat{R}_t$ is design of ice thickness of the tower. In this paper, ZB straight tower, a tower of Chinese standards, is applied to test system, with $\hat{R}_{\mathrm{t}}=20$ [40].

With fault probability models (14)–(17), joint physical and cyber fault probabilities of a certain branch are given.

$$P_{\mathrm{err}}^{\mathrm{P}}=1-\prod_{i=1}^{G}(1-\lambda_{\mathrm{F}}^{i})(1-\lambda_{\mathrm{D}}^{i})(1-\lambda_{\mathrm{C}}^{i}),\tag{18}$$

$$P_{\mathrm{err}}^{\mathrm{C}}=1-\prod_{i=1}^{G}(1-\lambda_{\mathrm{D}}^{i})(1-\lambda_{\mathrm{C}}^{i})\tag{19}$$

where $G$ is the number of both physical units and cyber units of a certain branch. It is worth noting that for a certain branch, physical faults and cyber faults can occur individually or simultaneously, which depend on the fault state of physical and cyber units, respectively. For a certain physical unit and cyber unit at the same location, the same tower element and $\lambda_{\mathrm{C}}^{i}$ are shared. However, since $\hat{R}_{\mathrm{w}}$ differs from cyber network wires to physical wires, $\lambda_{\mathrm{D}}^{i}$ is not the same.

## B. Cyber-physical Response Model

*1) Response Process*

Figure 8 depicts the cyber-physical coupling structure of a transmission network using OPGW. For the physical layer, the power transmission branch between bus 1 and bus 2 consists merging units (blue) and control units (yellow) at both ends of the branch. For the cyber layer, since communication network is established over the physical transmission branch, it has the same topology with physical network. After measuring electrical signals, sensors in the merging unit send data to the control center.

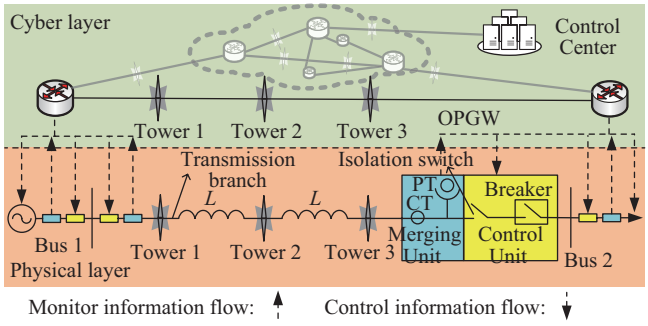


Fig. 8. Monitoring and control functions of a cyber-physical branch.

Faults that occur on physical branches, such as short-circuit faults or branch flow violation, are cut off by a protective relay protection automatically. Then, the control center receives fault information and calculates response strategy (detailed in Section IV-B3), with control commands sent to corresponding control units. Faults that occur on cyber branches do not directly lead to any physical fault or response strategy, but when parts of physical system are affected by an ice storm, cyber faults may cause physical faults and lead to more severe load shedding [41].

ES systems are added to enhance system resilience. When there is a power shortage caused by physical islanding, unmonitorable faults due to cyber disconnected, ramping constraints, flow constraints, etc., ES systems fill the shortage with emergency power outputs.

*2) Cyber Faults Handling*

To assess impact of cyber faults on cyber-physical network, failure of monitoring and control are discussed.

Failure of monitoring: Monitoring is the means for the control center to discover the fault and carry out response strategy immediately. It is worth noting that equivalent treatments are needed during simulation: a) Due to the lack of hardware in the loop, actual power flow of each branch is essentially obtained by equivalent power flow calculation. b) For unmonitorable branch, upper limit of power flow is equivalently set as infinity, which is only used for blinding control center to make no-response when branch is overloaded. In reality, the unmonitorable physical branch still has original upper limit of power flow, and failure of monitoring does not affect physical trip when faults occur. c) The equivalent infinity setting is only used in the fault discovery process for control center. Once another monitorable branch is overloaded, upper limits used for the response strategy is the correct value.

Failure of control: Remote control of generators, branches and load is the follow-up step for the control center to make response strategy to faults. If part of cyber network is damaged, control objects become disconnected. Under such circumstances, manual mode including phone call, short message, e-mail becomes the only way to adjust objects. Undoubtedly, manual mode is much worse than the automatic mode on control speed and difficulty. For simplicity, only automatic mode is considered in this paper. Cyber disconnected objects become boundary conditions of response strategy, which means they either maintain state of last moment, or tripped by relay.

*3) Response Strategy*

The cyber-physical response strategy, an optimal model, is carried out when the system state changes, such as faults occur or branches finish repair. The objective function is to minimize the operation cost, which is shown as follows:

$$\begin{aligned}\min C_{t,s}^{\mathrm{System}}&=\min\left\{C_{t,s}^{\mathrm{ES}}+C_{t,s}^{\mathrm{g}}+C_{t,s}^{\mathrm{d}}\right\}\\&=\min\Bigg\{\sum_{i\in\mathcal{N}_{\mathrm{ES}}}c_{\mathrm{ES}}|P_{\mathrm{ES}}^{i}(t)|+\sum_{j\in\mathcal{N}_{\mathrm{g}}}c_{\mathrm{g}}P_{\mathrm{g}}^{j}(t)\\&\quad+\sum_{k\in\mathcal{N}_{\mathrm{d}}}c_{\mathrm{d}}\Delta P_{\mathrm{d}}^{k}(t)\Bigg\},\ \forall t\in T\end{aligned}\tag{20}$$

where $C_{t,s}^{\mathrm{ES}},C_{t,s}^{\mathrm{g}},C_{t,s}^{\mathrm{d}}$ are the cost of ES systems, generators and load shedding at time $t$ of scenario $s$, and $c_{\mathrm{ES}},c_{\mathrm{g}},c_{\mathrm{d}}$ are unit cost, and $P_{\mathrm{ES}}^{i}(t),P_{\mathrm{g}}^{j}(t),\Delta P_{\mathrm{d}}^{k}$ are activating power, respectively. There are three orders in (20), where $C_{t,s}^{\mathrm{g}}$ is

smallest, $C_{t,s}^{\mathrm{ES}}$ is second smallest and $C_{t,s}^{\mathrm{d}}$ is largest. Considering need for calculation speed, DC power flow is applied and cyber-physical response model is solved with mixed integer linear programming (MILP) algorithm, which is given as follows.

$$\boldsymbol{F}(\boldsymbol{S}(t)) = \boldsymbol{A}(\boldsymbol{S}(t))(\boldsymbol{P}_{\mathrm{ES}}(t) + \boldsymbol{P}_{\mathrm{g}}(t) - \boldsymbol{P}_{\mathrm{d}}(t) + \Delta\boldsymbol{P}_{\mathrm{d}}(t)) \tag{21}$$

$$\sum_{i\in\mathcal{N}_{\mathrm{ES}}} P_{\mathrm{ES}}^{i}(t) + \sum_{j\in\mathcal{N}_{\mathrm{g}}} P_{\mathrm{g}}^{j}(t) = \sum_{k\in\mathcal{N}_{\mathrm{d}}} P_{\mathrm{d}}^{k}(t) - \sum_{k\in\mathcal{N}_{\mathrm{d}}} \Delta P_{\mathrm{d}}^{k}(t) \tag{22}$$

$$-P_{\mathrm{ES\_plan}}^{i} \le P_{\mathrm{ES}}^{i}(t) \le P_{\mathrm{ES\_plan}}^{i},\ i \in \mathcal{N}_{\mathrm{ES}} \tag{23}$$

$$SOC_{\mathrm{ES}}^{i}(t) = SOC_{\mathrm{ES}}^{i}(t-1) - P_{\mathrm{ES}}^{i}(t)\Delta t / E_{\mathrm{ES}}^{i},\ i \in \mathcal{N}_{\mathrm{ES}} \tag{24}$$

$$SOC_{\mathrm{ES\_min}}^{i} \le SOC_{\mathrm{ES}}^{i}(t) \le SOC_{\mathrm{ES\_max}}^{i},\ i \in \mathcal{N}_{\mathrm{ES}} \tag{25}$$

$$x(t)P_{\mathrm{g\_min}}^{j} \le P_{\mathrm{g}}^{j}(t) \le x(t)P_{\mathrm{g\_max}}^{j},\ j \in \mathcal{N}_{\mathrm{g}}^{\mathrm{c}}(t) \tag{26}$$

$$\begin{aligned} P_{\mathrm{g}}^{j}(t) - P_{\mathrm{g}}^{j}(t-1) \le{}& [2 - x(t-1) - x(t)]P_{\mathrm{g\_min}}^{j} \\ &+[1 + x(t-1) - x(t)]R_{\mathrm{g\_up}}^{j},\ j \in \mathcal{N}_{\mathrm{g}}^{\mathrm{c}}(t) \end{aligned} \tag{27}$$

$$\begin{aligned} P_{\mathrm{g}}^{j}(t-1) - P_{\mathrm{g}}^{j}(t) \le{}& [2 - x(t-1) - x(t)]P_{\mathrm{g\_max}}^{j} \\ &+[1 - x(t-1) + x(t)]R_{\mathrm{g\_down}}^{j},\ j \in \mathcal{N}_{\mathrm{g}}^{\mathrm{c}}(t) \end{aligned} \tag{28}$$

$$P_{\mathrm{g}}^{j}(t) = y(t)P_{\mathrm{g}}^{j}(t-1),\ j \in \mathcal{N}_{\mathrm{g}}^{\mathrm{u}}(t) \tag{29}$$

$$0 \le \Delta P_{\mathrm{d}}^{k} \le P_{\mathrm{d}}^{k},\ k \in \mathcal{N}_{\mathrm{d}}^{\mathrm{c}}(t) \tag{30}$$

$$\Delta P_{\mathrm{d}}^{k}(t) = z(t)\Delta P_{\mathrm{d}}^{k}(t-1),\ k \in \mathcal{N}_{\mathrm{d}}^{\mathrm{u}}(t) \tag{31}$$

$$|F^{l}(\boldsymbol{S}(t))| \le F_{\max}^{l},\ l \in \mathcal{N}_{\mathrm{b}} \tag{32}$$

where (21) is power flow constraint and $\boldsymbol{F}(\boldsymbol{S}(t))$, $\boldsymbol{P}_{\mathrm{ES}}(t)$, $\boldsymbol{P}_{\mathrm{g}}(t)$, $\boldsymbol{P}_{\mathrm{d}}(t)$, $\Delta\boldsymbol{P}_{\mathrm{d}}(t)$ are the active power flow vector, active power injection vector of ES systems, generators, active power consuming vector of load, and shedding vector of load at time $t$ respectively. $\boldsymbol{A}(\boldsymbol{S}(t))$ is Power Transfer Distribution Factors (PTDF) matrix of system, representing the relationship between active power flow of fault state $\boldsymbol{S}(t)$ and injected power of buses. $\mathcal{N}_{\mathrm{ES}}, \mathcal{N}_{\mathrm{g}}, \mathcal{N}_{\mathrm{d}}, \mathcal{N}_{\mathrm{b}}$ are sets of ES systems, generators, load and branches. $\mathcal{N}_{\mathrm{g}}^{\mathrm{c}}$, $\mathcal{N}_{\mathrm{g}}^{\mathrm{u}}$, $\mathcal{N}_{\mathrm{d}}^{\mathrm{c}}$, $\mathcal{N}_{\mathrm{d}}^{\mathrm{u}}$ are sets of controllable and uncontrollable generators and load, where $\mathcal{N}_{\mathrm{g}}^{\mathrm{c}} \cup \mathcal{N}_{\mathrm{g}}^{\mathrm{u}} = \mathcal{N}_{\mathrm{g}}$ and $\mathcal{N}_{\mathrm{d}}^{\mathrm{c}} \cup \mathcal{N}_{\mathrm{d}}^{\mathrm{u}} = \mathcal{N}_{\mathrm{d}}$. (22) is power balance constraint. (23)–(25) are constraints of ES systems, where $SOC_{\mathrm{ES}}^{i}(t)$ is state of charge at time $t$ and $E_{\mathrm{ES}}^{i}$ is capacity. (26)–(29) are power constraints of generators, where $P_{\mathrm{g\_min}}^{j}$ and $P_{\mathrm{g\_max}}^{j}$ are the minimum and maximum output of generator $j$. $R_{\mathrm{g\_up}}^{j}$ and $R_{\mathrm{g\_down}}^{j}$ are the ramp rate. $x(t) = \{1, 0\}$ represents the on/off state, with which startup and shutdown state and the ramping character can be described in a same formula. $y(t) = \{1, 0\}$ denotes the uncontrollable generator either maintains the last state or is cut by relay. (30)–(31) are constraints of load, where $z(t) = \{1, 0\}$ represents uncontrollable load either maintains last state or is cut by relay. (32) is power constraint of branch where $F_{\max}^{l}$ is the maximum power flow of branch $l$.

### C. Restoration Model

For each fault unit, the repair team starts from the repair center, and moves to the fault point. After restoration, they return to repair center. The following is considered during restoration process.

#### 1) Meteorological Condition

Different disaster intensity corresponds to different repair time, which has a positive correlation.

$$T_{\mathrm{total}}^{i} = T_{\mathrm{repair}}^{i} + T_{\mathrm{wait}}^{i} = T_{\mathrm{repair}}^{i\_\mathrm{normal}} \cdot k + T_{\mathrm{wait}}^{i} \tag{33}$$

where $T_{\mathrm{repair}}^{i}$ represents repair time of fault point $i$, and $T_{\mathrm{wait}}^{i}$ is waiting time for the idle repair team. Moreover, $T_{\mathrm{repair}}^{i\_\mathrm{normal}}$ is repair time under normal weather, and $k$ is the corresponding weather impact factor, which is related to ice thickness $R$ shown as follows.

$$k = \begin{cases} 1, & 0 \le R < 10 \\ \mathrm{rand}(1,2), & 10 \le R < 20 \\ \mathrm{rand}(2,3), & 20 \le R < 30 \\ \mathrm{rand}(3,4), & 30 \le R < 40 \\ \mathrm{rand}(4,5), & 40 \le R < 50 \end{cases} \tag{34}$$

#### 2) Distance

Due to large span of transmission network, repair time includes two parts:

$$T_{\mathrm{repair}}^{i\_\mathrm{normal}} = T_{\mathrm{work}}^{i\_\mathrm{normal}} + T_{\mathrm{road}}^{i\_\mathrm{normal}} \tag{35}$$

where $T_{\mathrm{work}}^{i\_\mathrm{normal}}$ is repair working time and $T_{\mathrm{road}}^{i\_\mathrm{normal}}$ is time spent on road between fault point and repair center.

#### 3) Cyber-Physical Characteristic

When OPGW is under repair, transmission line has to be disconnected to ensure safety of engineers. Besides, if both cyber and physical units fail, cyber unit is repaired first.

## V. Two-Stage Problem Formulation

Figure 9 summarizes cyber-physical resilience enhancement of Section III and IV, considering full life cycle of ice storm. In Fig. 9, the main process is shown in the middle column, including planning of ES systems before ice storm (Stage 1, Section III) and the resilient process with ES systems during ice storm (Stage 2, Section IV).

To avoid dimension disaster and reduce solving time of Stage 1, objective function (10) is simplified as:

$$\min\left\{C_{\mathrm{ES}}^{\mathrm{plan}} + \sum_{s\in\Omega_s} P_s \max_{t\in T}\left[\min\left(k_{\mathrm{g}} \cdot C_{t,s}^{\mathrm{System}}\right)\right]\right\} \tag{36}$$

where the first $\min$ is to minimize the total cost. The $\max$ is to find out the most serious time of the whole disaster of each scenario. The second $\min$ is to ensure the minimum cost at the most serious time.

The whole two-stage optimal problem is described as:

$$\text{Stage 1}: \begin{cases} \text{object (36)} \\ \text{s.t. (11)–(13), (21)–(23), (26)–(32)} \end{cases} \tag{37}$$

$$\text{Stage 2}: \begin{cases} \text{object (20)} \\ \text{s.t. (21)–(32)} \end{cases} \tag{38}$$

To solve such problems, the Monte Carlo method is applied to simulate multiple scenarios of cyber-physical resilient process under ice storm, in which occurrence of ice storm (6) and fault (14)–(17) can be determined by sampling probability of them appearing in each state.

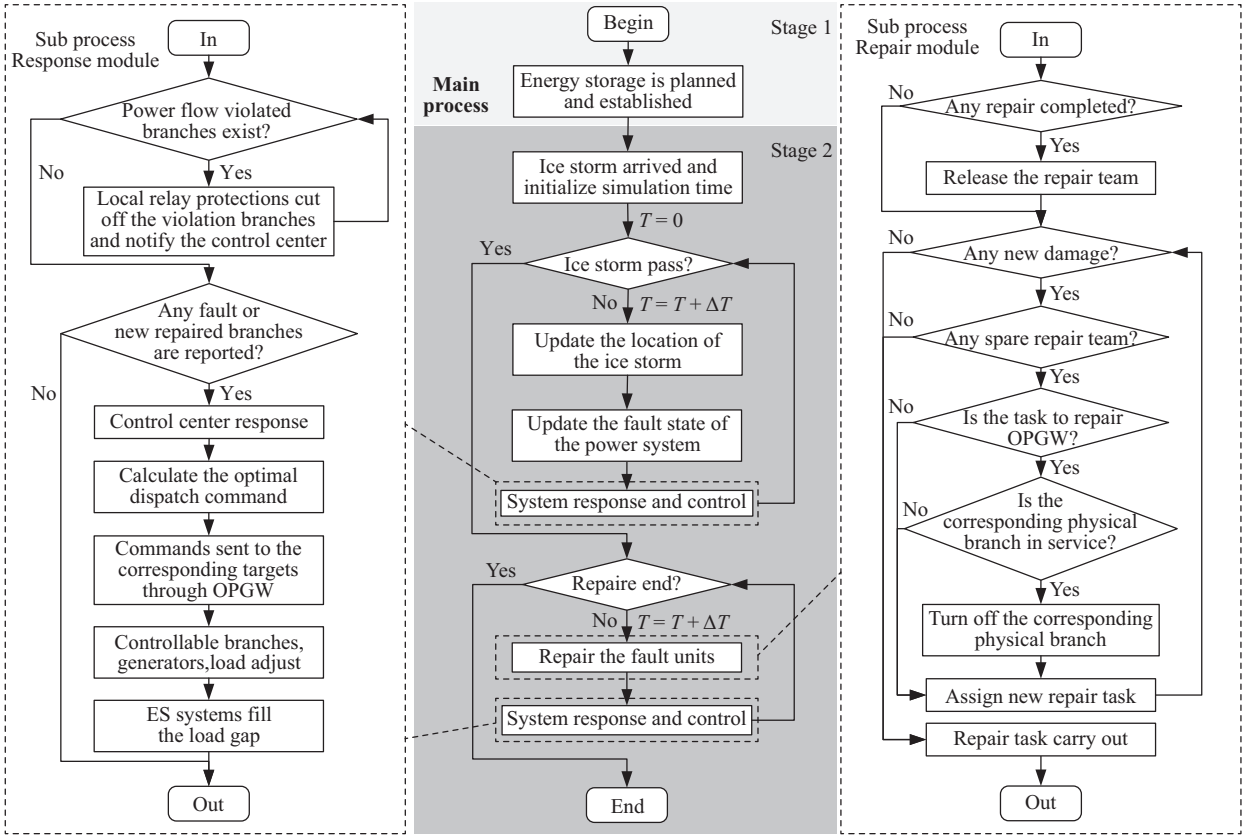


Fig. 9. Flowchart of cyber-physical resilient process considering full life cycle of the ice storm.

## VI. Simulation

In this section, the proposed model is verified in IEEE RTS-79 with Python 3.11 and Gurobi 9.1.1. There are 32 generators in IEEE RTS-79, and initial load of the system is 2850 MW. Simulation time step is 0.01 h, which balances accuracy and simulation speed. Monte Carlo simulation times is 1000. $k_{\mathrm{g}} = 10^8$, $E^{i}_{\mathrm{ES\_max}} = 3200$ and 0.125 C battery is considered, which means battery can be fully charged within 8 hours. With such configurations, $C_{\mathrm{fix}} = 10^6$, $C_{\mathrm{cap}} = 1.5 \times 10^6$. The following parameters of ice storm are assumed to obey normal probability distributions, where $V_{\max} \sim N(12, 1^2)$, $r_{\max} \sim N(100, 0.5^2)$, $P_{\max} \sim N(35, 1^2)$, $V_{\mathrm{m}} \sim N(20, 0.5^2)$, $\delta \sim N(\pi/4, 0.1^2)$ and landing site coordinate is assumed to obey a uniform probability distribution $(x_0, y_0) = (x, 670-x)$, where $x \sim U(220{,}240)$. The control center and restoration center are located at node 8 and bus 3. $T^{i\_\mathrm{normal}}_{\mathrm{work}} = 1$, $T^{i\_\mathrm{normal}}_{\mathrm{road}} = 2D/v$, where $D$ is distance between fault point and bus 3, and $v = 60$ is moving speed of engineers.

The resilient process of cyber-physical transmission network is tested in six cases shown in Table I.

### A. Stage 1 Results

In case $S_3$ and $S_5$ of Table I, ES systems are set at buses with largest load. In case $S_4$ and $S_6$, ES systems are planned according to optimal model. Allocation results and cost of first stage are shown in Table II, where $C^{\mathrm{plan}}_{\mathrm{System}} = \sum_{s\in\Omega_s} P_s \max_{t\in T}[\min(k_{\mathrm{g}} \cdot C^{\mathrm{System}}_{t,s})]$.

TABLE I
Setting of Different Cases

| Case | CPS | ES | Planning | Case | CPS | ES | Planning |
|---|---|---|---|---|---|---|---|
| $S_1$ | ✗ | ✗ | ✗ | $S_4$ | ✗ | ✓ | ✓ |
| $S_2$ | ✓ | ✗ | ✗ | $S_5$ | ✓ | ✓ | ✗ |
| $S_3$ | ✗ | ✓ | ✗ | $S_6$ | ✓ | ✓ | ✓ |

TABLE II
Allocation Results of ES Systems

| Case | Location | $E_{\mathrm{ES}}$ (MWh) | $C^{\mathrm{plan}}_{\mathrm{ES}}$ (CNY) | $C^{\mathrm{plan}}_{\mathrm{System}}$ (CNY) |
|---|---|---|---|---|
| $S_3S_5$ | Bus 13<br>Bus 15<br>Bus 18 | 1060<br>1268<br>1332 | $5.49 \times 10^9$ | $S_3 : 6.65 \times 10^6$<br>$S_5 : 7.30 \times 10^6$ |
| $S_4S_6$ | Bus 3<br>Bus 14<br>Bus 19 | 720<br>776<br>724 | $3.33 \times 10^9$ | $S_4 : 1.25 \times 10^6$<br>$S_6 : 2.21 \times 10^6$ |

Results show that $S4$, $S6$ have lower cost of $C^{\mathrm{plan}}_{\mathrm{ES}}$, $C^{\mathrm{System}}_{t,s}$ than $S3$, $S5$. In $S4$, $S6$, according to distribution probability of ice storms, bus 14, 19, 24 have high islanding probability, thus setting ES systems at these buses can reduce load shedding. On the other hand, in $S3$, $S5$, installing ES systems at bus 13, 15, 18 leads to waste and has little use in enhancing resilience of the system.

Moreover, when ES systems are set at the same location, cases only consider the physical characteristic ($S3$, $S4$) have smaller $C^{\mathrm{System}}_{t,s}$ than cyber-physical cases ($S5$, $S6$). Because there is no failure of monitoring and control, and more generators are used rather than ES systems.

### B. Stage 2 Results

To assess resilience of cases in Table I, average load curve calculated by Monte Carlo sampling method is depicted in Fig. 10. Comparison analyses are given:

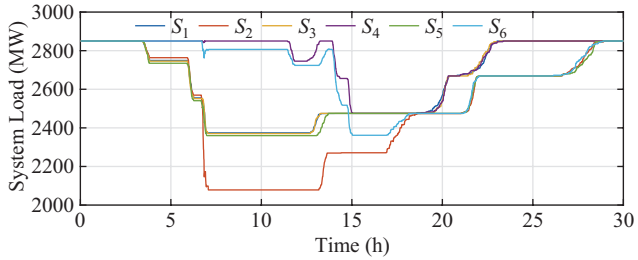


Fig. 10. Average system load curves.

1) Comparison on CPS characteristics. As shown in Fig. 10, it can be found between $S_1$ and $S_2$, $S_3$ and $S_5$, $S_4$ and $S_6$ when the cyber-physical characteristic is considered, the resilience of the system gets worse. The system load of $S_2$ is much lower than $S_1$ during 7–17 h. It is because there is no ES and cyber faults indirectly destroy system and lead to heavier load shedding. Similar results can be found in comparison between $S_3$ and $S_5$, $S_4$ and $S_6$.

2) Comparison of ES systems. As shown in Fig. 10, it can be found between $S_1$ and $S_3$, $S_2$ and $S_5$ that the resilience is improved by ES only when CPS characteristic is considered. The reason is when the failure of cyber network is not considered, generators connected by a cyber network to the control center are regarded as adjustable. According to (20), there is no space for ES to generate, which leads to the almost same load curve of $S_1$ and $S_3$. However, for $S_2$ and $S_5$ when CPS is considered, ES enhances system resilience.

3) Comparison on planning of ES systems. As shown in Fig. 10, it can be found between $S_3$ and $S_4$, $S_5$ and $S_6$, when ES systems are allocated at proper places, effect of enhancement is better. The system load of $S_3$ is much lower than $S_4$ during 4–17 h. Similar results can be found in comparison between $S_5$ and $S_6$. When ES systems are planned, beginning time of load shedding has been effectively postponed ($S_4$, $S_6$ vs $S_1$, $S_2$, $S_3$, $S_5$). At about 15 h, when ES systems are flat and faults have not been repaired, load shedding occurs. It is worthy of note the curve of $S_6$ leads to an even worse state than $S_5$ at 15 h, because at the early stage of the ice storm (3–10 h) large load shedding does not occur, and generators are still with a high power output. When ES systems run out, there is no adjustment space for controllable generators. Besides, cyber faults disconnect parts of generators from control center. The above two reasons lead to additional load shedding of $S_6$ than $S_5$ during 15–18 h.

Additionally, corresponding indexes are given in Table III. Similar results can be found in comparison of CPS, ES systems and planning of ES systems.

The system load of a single Monte Carlo simulation is depicted in Fig. 11. Compared with Fig. 10, since iteration is 1, curves are less smooth. A single simulation of $S_6$ is taken as an example for analysis. At 0.12 h system affected by ice storm, and at 9.89 h ice storm departs. Fig. 12 depicts

TABLE III
AVERAGE RESILIENT INDEXES

| Case | $R_t$ (MWh) | $R_r$ | $R_{RICD}$ | Case | $R_t$ (MWh) | $R_r$ | $R_{RICD}$ |
|---|---|---|---|---|---|---|---|
| $S_1$ | 6416 | 0.872 | 0.397 | $S_4$ | 2622 | 0.918 | 0.424 |
| $S_2$ | 10554 | 0.836 | 0.307 | $S_5$ | 7948 | 0.881 | 0.317 |
| $S_3$ | 6455 | 0.871 | 0.397 | $S_6$ | 4653 | 0.917 | 0.334 |

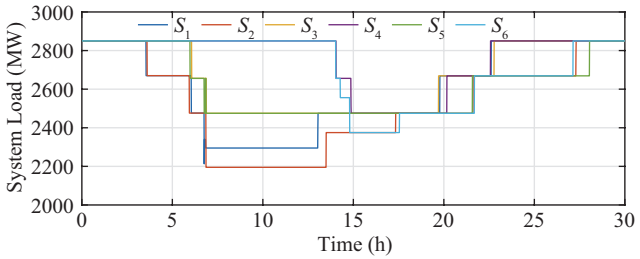


Fig. 11. System load curves of a single sample.

the system state of worst time 9.89 h. High fault similarity can be found in faults of cyber and physical networks, making the island area also a disconnected area. Due to ES systems, the first load shedding time is delayed to 14.03 h. System loads are 2850, 2656, 2556, 2375, 2475, 2669, 2850 MW at 0, 14.03, 14.28, 14.80, 17.55, 21.69, 27.14 h, respectively.

Corresponding events of the above case are listed in Table IV. Results show that the control center responses at each monitor-able physical branch changing moment. Controllable generators adjust for physical faults and there is no load shedding at 2.85, 3.23, 5.90 h. However, at 6.03, 6.77, 6.82 h controllable generators can not support the load and ES systems automatically fill up the gap. At 13.31, 15.93 h etc, when

TABLE IV
EVENTS OF $S_6$ OF A SINGLE SAMPLE

| Time | Branch | Strategy | Time | Branch | Strategy |
|---|---|---|---|---|---|
| 2.53 | ×2(c) | – | 13.31 | ✓2(c&p) | Response, $P_{ES}^{3}=0$ |
| 2.85 | ×2(p) | Response | 14.03 | $E_{ES}^{14}=0$ | Response, $P_{ES}^{14}=0$ |
| 2.89 | ×6(c) | – | 14.28 | !27(p) | Response |
| 3.15 | ×27(c) | – | 14.80 | $E_{ES}^{19}=0$ | Response, $P_{ES}^{19}=0$ |
| 3.23 | ×6(p) | Response | 15.93 | ✓6(c&p) | Response |
| 5.60 | ×19(c) | – | 17.55 | ✓27(c&p) | Response |
| 5.69 | ×23(c) | – | 17.97 | !31(p) | Response |
| 5.90 | ×19(p) | Response | 21.63 | ✓19(c) | – |
| 6.03 | ×23(p) | Response, $P_{ES}^{14}=194$ | 21.69 | ✓19(p) | Response |
| 6.46 | ×34(c) | – | 22.79 | ✓23(c&p) | Response |
| 6.51 | ×29(c) | – | 27.14 | ✓29(c&p) | Response |
| 6.53 | ×35(c) | – | 27.25 | !38(p) | Response |
| 6.77 | ×29(p), ×34(p) | Response, $P_{ES}^{3}=11$, $P_{ES}^{19}=160$ | 32.12 | ✓34(c&p) | Response |
| 6.78 | – | Response, $P_{ES}^{3}=0$, $P_{ES}^{19}=46$ | 32.77 | ✓31(c&p) | Response |
| 6.82 | ×35(p) | Response, $P_{ES}^{3}=11$, $P_{ES}^{19}=181$ | 37.98 | ✓35(c&p) | Response |
| 9.53 | ×38(c) | – | 40.02 | ✓38(c&p) | Response |
| 9.73 | ×31(c) | – | – | – | – |

Note: c: cyber, p: physical, ×: fault, ✓: repaired, !: turn off.

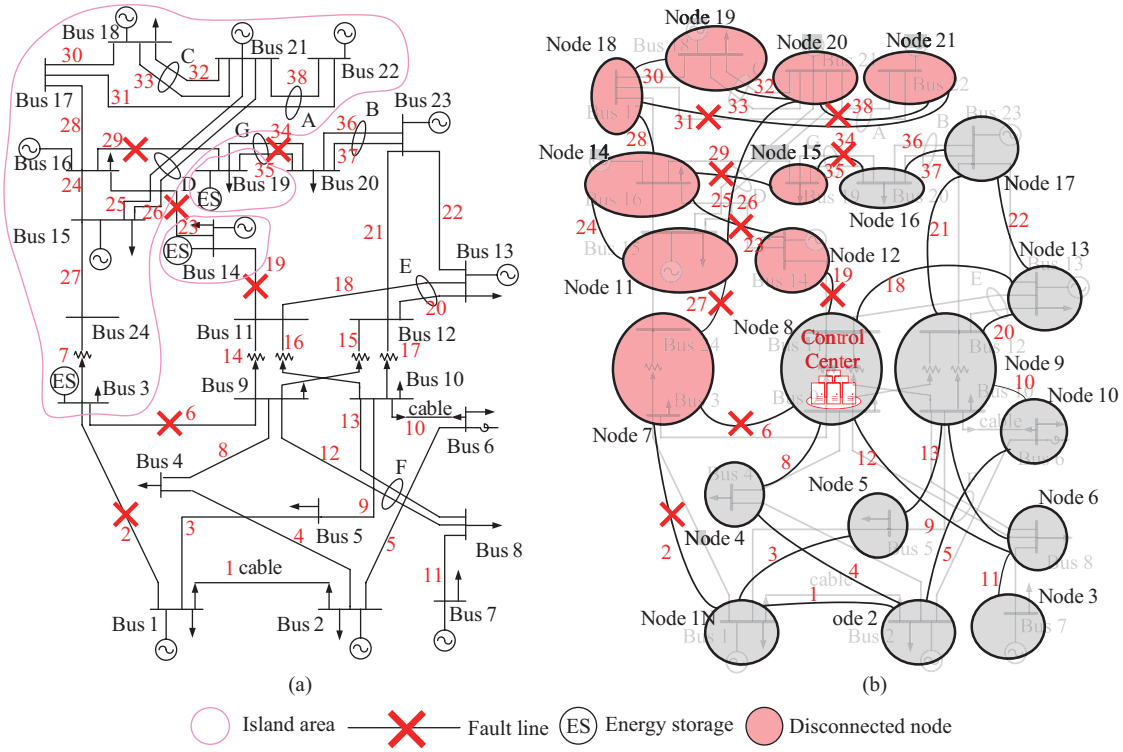


Fig. 12. System state of $S_6$ of a single sample ($t = 9.89$ h, ice storm departure time). (a) Physical network. (b) Cyber network.

some of cyber and physical branches finish restoration and the control center adjusts generators to restore power supply. At 14.03, 14.80 h when ES systems are flat, inevitable load shedding occurs. At 17.97, 27.25 h the cyber branch is under repair, the corresponding physical branch has to be turned off manually, which may lead to secondary load shedding of the system.

The operation cost of the second stage is shown in Fig. 13. It can be found that the total system operation cost $C^{\text{System}}$ is related to the load curve in Fig. 10 and corresponding indexes in Table III. The larger $C^{\text{System}}$ is, the worse the system is. Besides, $C^{\text{g}}$, $10C^{\text{ES}}$ and $C^{\text{d}}$ are given. Since most of the load is supplied by generators, $C^{\text{g}}$ differs a little. Due to the planning model of ES systems, $C^{\text{d}}$ reduces effectively in $S_4, S_6$ and the reduced part is supplied by $C^{\text{ES}}$, which verifies the order of objective function (20).

For further analysis, the average operation cost and power output of $S_6$ are given in Figs. 14 and 15 respectively. Results show that at the beginning of ice storm, all loads can be

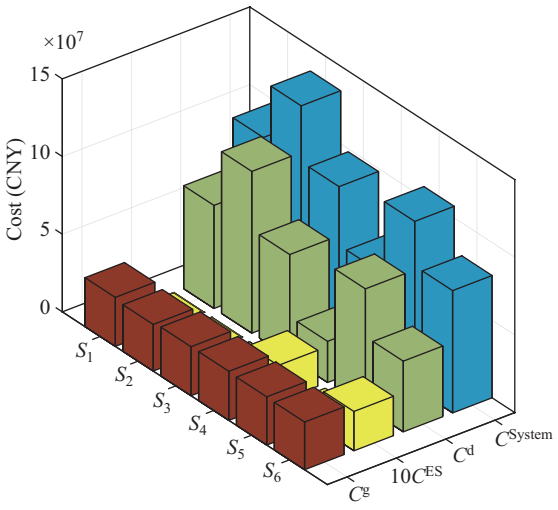


Fig. 13. Average operation costs.

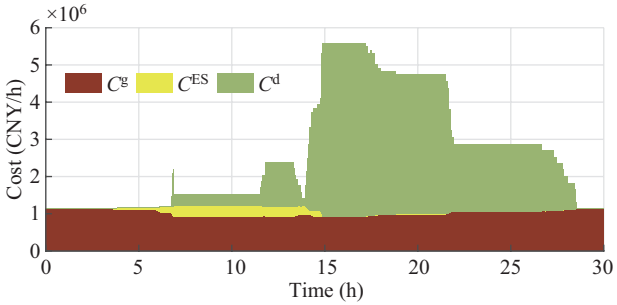


Fig. 14. Average operation costs of $S_6$.

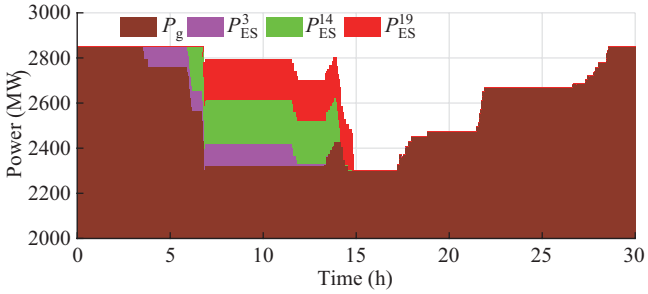


Fig. 15. Average power output of $S_6$.

supplied by generators. As faults increase, ES systems fill up load shortage to minimize $C^{\mathrm{System}}$ especially $C^{\mathrm{d}}$. When ES systems run out, $P_{\mathrm{ES}}$ turns to 0 and a large scale of load shedding occurs, with $C^{\mathrm{d}}$ increasing rapidly. When restoration is completed, $P_{\mathrm{g}}$ increases and $C^{\mathrm{d}}$ decreases. Fig. 14, 15 describe the resilient process from two perspective, which verify accuracy of the proposed cyber-physical resilience and its enhancement.

## VII. Conclusion

In this paper, a two-stage cyber-physical resilience enhancement method for transmission networks is proposed and verified. The first stage is planning of ES systems and the second stage is the cyber-physical resilient process considering ES systems. The main findings are as follows.

1) For the first stage, ES systems are installed according to the optimal planning model. A proper planning scheme can effectively improve resilience of the system and reduce the total operation cost during ice storm.

2) For the second stage, the proposed cyber-physical resilient process with ES systems is carried out under scenarios generated by joint PDF of ice storm parameters. The cyber-physical fault, response and restoration models are given and simulated. Results show when cyber faults occur, power supply is seriously affected, which reflects from the side that physical-only resilience assessment is inadequate and ES systems are efficient back-up resources under cyber faults.

For our future work, advanced enhancement with ES systems such as a proactive strategy, will be further studied.

## References


[1] S. L. Cutter, L. Barnes, M. Berry, C. Burton, E. Evans, E. Tate, and J. Webb, "A place-based model for understanding community resilience to natural disasters," *Global Environmental Change*, vol. 18, no. 4, pp. 598–606, Oct. 2008.

[2] A. Rose, "Economic resilience to natural and man-made disasters: Multidisciplinary origins and contextual dimensions," *Environmental Hazards*, vol. 7, no. 4, pp. 383–398, Jan. 2007.

[3] A. R. Berkeley III and M. Wallace, "A framework for establishing critical infrastructure resilience goals, final report and recommendations by the Council," National Infrastructure Advisory Council, Oct. 2010.

[4] T. Ding, M. Qu, Z. K. Wang, B. Chen, C. Chen, and M. Shahidehpour, "Power system resilience enhancement in typhoons using a three-stage day-ahead unit commitment," *IEEE Transactions on Smart Grid*, vol. 12, no. 3, pp. 2153–2164, May 2021.

[5] M. Y. Yan, M. Shahidehpour, A. Paaso, L. X. Zhang, A. Alabdulwahab, and A. Abusorrah, "Distribution system resilience in ice storms by optimal routing of mobile devices on congested roads," *IEEE Transactions on Smart Grid*, vol. 12, no. 2, pp. 1314–1328, Mar. 2021.

[6] D. N. Trakas and N. D. Hatziargyriou, "Optimal distribution system operation for enhancing resilience against wildfires," *IEEE Transactions on Power Systems*, vol. 33, no. 2, pp. 2260–2271, Mar. 2018.

[7] J. Bao, X. Wang, Y. H. Zheng, F. Zhang, X. Y. Huang, P. Sun, and Z. Y. Li, "Resilience-oriented transmission line fragility modeling and real-time risk assessment of thunderstorms," *IEEE Transactions on Power Delivery*, vol. 36, no. 4, pp. 2363–2373, Aug. 2021.

[8] Z. W. Shi, X. Y. Tan, H. Y. Li, H. Lin, J. Liu, and X. G. Lin, "Quantitative study on the waterlogging resilience of road transportation system based on the validity view of system functions," *Journal of Engineering Science and Technology Review*, vol. 12, no. 1, pp. 117–125, Feb. 2019.

[9] A. Mate, T. Hagan, E. Cotilla-Sanchez, T. K. A. Brekken, and A. Von Jouanne, "Impacts of earthquakes on electrical grid resilience," in *Proceedings of the IEEE/IAS 57th Industrial and Commercial Power Systems Technical Conference (I & CPS)*, 2021, pp. 1–5.

[10] M. Panteli, P. Mancarella, D. N. Trakas, E. Kyriakides, and N. D. Hatziargyriou, "Metrics and quantification of operational and infrastructure resilience in power systems," *IEEE Transactions on Power Systems*, vol. 32, no. 6, pp. 4732–4742, Nov. 2017.

[11] M. Panteli, C. Pickering, S. Wilkinson, R. Dawson, and P. Mancarella, "Power system resilience to extreme weather: Fragility modeling, probabilistic impact assessment, and adaptation measures," *IEEE Transactions on Power Systems*, vol. 32, no. 5, pp. 3747–3757, Sep. 2017.

[12] Y. H. Yang, W. H. Tang, Y. Liu, Y. L. Xin, and Q. H. Wu, "Quantitative resilience assessment for power transmission systems under typhoon weather," *IEEE Access*, vol. 6, pp. 40747–40756, Jul. 2018.

[13] M. Rahnamay-Naeini and M. M. Hayat," Cascading failures in interdependent infrastructures: An interdependent markov-chain approach," *IEEE Transactions on Smart Grid*, vol. 7, no. 4, pp. 1997–2006, Jul. 2016.

[14] C. Wang, Y. H. Hou, F. Qiu, S. B. Lei, and K. Liu, "Resilience enhancement with sequentially proactive operation strategies," *IEEE Transactions on Power Systems*, vol. 32, no. 4, pp. 2847–2857, Jul. 2017.

[15] C. Wang, P. Ju, S. B. Lei, Z. Y. Wang, F. Wu, and Y. H. Hou, "Markov decision process-based resilience enhancement for distribution systems: An approximate dynamic programming approach," *IEEE Transactions on Smart Grid*, vol. 11, no. 3, pp. 2498–2510, May 2020.

[16] X. N. Liu, K. Hou, H. J. Jia, J. B. Zhao, L. Mili, X. L. Jin, and D. Wang, "A planning-oriented resilience assessment framework for transmission systems under typhoon disasters," *IEEE Transactions on Smart Grid*, vol. 11, no. 6, pp. 5431–5441, Nov. 2020.

[17] K. Tierney and M. Bruneau, "Conceptualizing and measuring resilience: A key to disaster loss reduction," *TR News: Transportation Research*, no. 250, pp. 14–15, 17, May 2007.

[18] J. Kim and Y. Dvorkin, "Enhancing distribution system resilience with mobile energy storage and microgrids," *IEEE Transactions on Smart Grid*, vol. 10, no. 5, pp. 4996–5006, Sep.2019.

[19] Y. Wang, A. O. Rousis, and G. Strbac, "Resilience-driven optimal sizing and pre-positioning of mobile energy storage systems in decentralized networked microgrids," *Applied Energy*, vol. 305, pp. 117921, Jan. 2022.

[20] G. Zhang, F. Zhang, X. Zhang, Z. Y. Wang, K. Meng, and Z. Y. Dong, "Mobile emergency generator planning in resilient distribution systems: A three-stage stochastic model with nonanticipativity constraints," *IEEE Transactions on Smart Grid*, vol. 11, no. 6, pp. 4847–4859, Nov. 2020.

[21] S. B. Lei, C. Chen, Y. Song, and Y. H. Hou, "Radiality constraints for resilient reconfiguration of distribution systems: Formulation and application to microgrid formation," *IEEE Transactions on Smart Grid*, vol. 11, no. 5, pp. 3944–3956, Sep. 2020.

[22] S. H. Yao, P. Wang, and T. Y. Zhao, "Transportable energy storage for more resilient distribution systems with multiple microgrids," *IEEE Transactions on Smart Grid*, vol. 10, no. 3, pp. 3331–3341, May 2019.

[23] S. H. Yao, P. Wang, X. C. Liu, H. J. Zhang, and T. Y. Zhao, "Rolling optimization of mobile energy storage fleets for resilient service restoration," *IEEE Transactions on Smart Grid*, vol. 11, no. 2, pp. 1030–1043, Mar. 2020.

[24] A. Arjomandi-Nezhad, M. Fotuhi-Firuzabad, M. Moeini-Aghtaie, A. Safdarian, P. Dehghanian, and F. Wang, "Modeling and optimizing recovery strategies for power distribution system resilience," *IEEE Systems Journal*, vol. 15, no. 4, pp. 4725–4734, Dec. 2021.

[25] J. Guo, Y. Q. Han, C. X. Guo, D. H. Li, and J. B. Sun, "Reliability assessment of cyber physical power system considering monitoring function and control function," *Proceedings of the CSEE*, vol. 36, no. 8, pp. 2123–2130, Apr. 2016.

[26] J. M. Yan, J. B. Xu, M. Ni, and W. J. Yu, "Impact of communication system interruption on power system wide area protection and control system," *Automation of Electric Power Systems*, vol. 40, no. 5, pp. 17–24, Mar. 2016.

[27] L. Xu, Q. L. Guo, X. Z. Liu, and H. B. Sun, "Robust optimization method of communication network to improve resilience of cyber-physical power system," *Automation of Electric Power Systems*, vol. 45, no. 3, pp. 68–75, Feb. 2021.

[28] T. H. Liu, R. J. Sun, Y. T. Liu, and C. Y. Wang, "A resilience enhancement scheme of cyber-physical power system for extreme natural disasters," in *Proceedings of 2020 IEEE Sustainable Power and Energy Conference (iSPEC)*, 2020, pp. 1684–1689.

[29] K. Y. Pang, Y. Z. Wang, F. Q. Wang, C. Y. Wang, J. H. Zhao, and Y. L. Liu, "Cyber- physical collaborative restoration strategy for power transmission system with communication failures," *Automation of Electric Power Systems*, vol. 45, no. 3, pp. 58–67, Feb. 2021.

[30] L. Xu, Q. L. Guo, Y. J. Sheng, S. M. Muyeen, and H. B. Sun, "On the resilience of modern power systems: A comprehensive review from

the cyber- physical perspective," *Renewable and Sustainable Energy Reviews*, vol. 152, pp. 111642, Dec. 2021.
[31] K. Jalilpoor, M. T. Ameli, S. Azad, and Z. Sayadi, "Resilient energy management incorporating energy storage system and network reconfiguration: A framework of cyber-physical system," *IET Generation, Transmission & Distribution*, vol. 17, no. 8, pp. 1734–1749, Apr. 2023.
[32] P. M. Subcommittee, "IEEE reliability test system," *IEEE Transactions on Power Apparatus and Systems*, vol. PAS-98, no. 6, pp. 2047–2054, Nov. 1979.
[33] R. Liu, C. Vellaithurai, S. S. Biswas, T. T. Gamage, and A. K. Srivastava, "Analyzing the cyber-physical impact of cyber events on the power grid," *IEEE Transactions on Smart Grid*, vol. 6, no. 5, pp. 2444–2453, Sep. 2015.
[34] W. H. Zhang, T. Qian, X. Lin, W. H. Tang, and Q. H. Wu, "Co-simulation for cyber-physical distribution network under cyber attacks," in *Proceedings of 2018 International Conference on Power System Technology (POW-ERCON)*, 2018, pp. 2996–3002.
[35] K. F. Jones, "A simple model for freezing rain ice loads," *Atmospheric Research*, vol. 46, no. 1–2, pp. 87–97, Apr. 1998.
[36] M. Bruneau and A. Reinhorn, "Exploring the concept of seismic resilience for acute care facilities," *Earthquake Spectra*, vol. 23, no. 1, pp. 41–62, Feb. 2007.
[37] M. Ouyang, L. Dueñas-Osorio, and X. Min, "A three-stage resilience analysis framework for urban infrastructure systems," *Structural Safety*, vol. 36–37, pp. 23–31, May/Jul. 2012.
[38] F. Yin, X. Jiang, M. Farzaneh, J. Hu, and Y. Liu, "Electrical performance of composite insulators under icing conditions," in *2012 Annual Report Conference on Electrical Insulation and Dielectric Phenomena*, 2012, pp. 815–818.
[39] S. W. Mei, A. C. Xue, and X. M. Zhang, *Selforganized Criticality of Power System and Securiry of Large Power Grid*. Beijing: Tsinghua University Press, 2009.
[40] F. C. Cao, *Transmission Line Tower Type Manual*. Beijing: China Electric Power Press, 2009.
[41] B. Falahati and Y. Fu, "A study on interdependencies of cyber-power networks in smart grid applications," in *Proceedings of 2012 IEEE PES Innovative Smart Grid Technologies (ISGT)*, 2012, pp. 1–8.

**Wenhao Zhang** obtained B.Eng. and Ph.D. degrees in Electrical Engineering from South China University of Technology (SCUT), Guangzhou, China, in 2016 and 2021, respectively. He is currently working as a Postdoctoral Researcher at SCUT and Guangzhou Zhiguang Electric Co., Ltd. His interests include cyber-physical power systems, energy storage systems and electricity markets.

**Dongyang Rui** obtained B.Eng. and M.Sc. degrees in Electrical Engineering from SCUT and Huazhong University of Science and Technology (HUST), respectively. He is the Vice President of Guangzhou Zhiguang Electric Co., Ltd and the Legal Representative of Zhiguang Research Institute (Guangzhou) Co., Ltd. Currently, he is working on the digitization of large-scale energy storage systems of China.

**Weihong Wang** obtained B.Eng. and M.Sc. degrees in Electrical Engineering from Tsinghua University, Beijing, China. He is currently the CTO of Zhiguang Research Institute (Guangzhou) Co., Ltd. His research interests include IoT, cloud computing, big data. He is now working on industrial internet, especially the modeling and control of large-scale energy storage systems.

**Yang Guo** obtained a Ph.D. degree in Computer Science from SCUT. He is currently the CIO of Zhiguang Research Institute (Guangzhou) Co., Ltd, leading his team in designing digital energy applications. He has developed multiple large-scale cloud platforms, including Industrial Internet platform, Smart Energy Storage platform, PV-ES-Charging-Microgrid Energy Management System. His research interests include AI, IoTs, edge computing and cloud computing on electric applications.

**Zhaoxia Jing** received B.Eng. and Ph.D. degrees in Electrical Engineering from HUST, Wuhan, China, in 1997 and 2003, respectively. She is currently a Professor with the School of Electric Power Engineering, South China University of Technology. Her research interests include electricity markets, integrated energy system optimization, and electric vehicles.

**Wenhu Tang** received B.Eng. and M.Sc. degrees in Electrical Engineering from Huazhong University of Science and Technology, Wuhan, China, in 1996 and 2000, respectively, and the Ph.D. degree in Electrical Engineering from The University of Liverpool, Liverpool, U.K., in 2004. He was a Postdoctoral Research Associate and subsequently a Lecturer at The University of Liverpool between 2004 and 2013. He is currently a distinguished professor and dean of School of Electric Power Engineering, South China University of Technology, Guangzhou, China. He has authored and coauthored more than 150 research papers and 1 Springer research monograph. His research interests include renewable energy integration in power grids, condition monitoring and fault diagnosis for power apparatus and power system resilience assessment.